Structural Studies of $NaPO_3$-AlF_3 Glasses by High-Resolution Double-Resonance NMR Spectroscopy

Henrik Bradtmüller[a], Long Zhang [a,b], Carla C. de Araujo[a], Hellmut Eckert [a,c*], Doris Möncke[d] and Doris Ehrt[e]

[a] Institut für Physikalische Chemie, Westfälische Wilhelms-Universität Münster, Corrensstr. 30, D-48149 Münster, Germany

[b] Shanghai Institute of Optics and Fine Mechanics, Chinese Academy of Sciences, P. O. Box: 800-211, 201800 Shanghai, China

[c] Instituto de Física São Carlos, Universidade de São Paulo, CP 369, São Carlos, SP 13566-590

[d] Theoretical and Physical Chemistry Institute, National Hellenic Research Foundation, 48 Vassileos Constantinou Avenue, 11635 Athens, Greece

[e] Otto-Schott-Institut, Friedrich-Schiller-Universität Jena, Fraunhoferstr. 6, D-07743 Jena, Germany

* Author to whom correspondence should be addressed.
Phone: 49-251-8329161; Fax: 49-251-8329159; E-mail: eckerth@uni-muenster.de.

Abstract

The local structure of the model glasses $(NaPO_3)_{1-x}$-$(AlF_3)_x$ ($0 \leq x \leq 0.4$), prepared by standard melt-cooling, was extensively investigated by high-resolution solid state NMR including advanced double resonance techniques. This glass system offers the opportunity of studying five different heteronuclear distance correlations (Na-F, Na-P, P-F, Al-F, P-Al) by ten distinct double resonance experiments, involving all of the constituent elements present. ^{27}Al MAS-NMR data indicate that aluminum is predominantly six-coordinated. According to ^{27}Al{^{31}P} and ^{27}Al{^{19}F} rotational echo double resonance (REDOR) spectroscopic results, two to three Al-F and three to four Al-O-P linkages occur in these glasses, independent of composition *x*. ^{19}F MAS-NMR spectra show the presence of terminal P-bound and Al-bound fluorine species. A small amount of fluorine bridging to two aluminum octahedra, which could be assigned based on ^{19}F{^{27}Al} and ^{19}F{^{31}P} REDOR experiments, was also detected. ^{19}F{^{23}Na} REDOR experiments indicate that the Al-bound terminal F atoms interact significantly more strongly with sodium ions than the P-bonded terminal F atoms, which is consistent with local charge considerations. Based on the detailed quantitative dipole-dipole coupling information obtained, a comprehensive structural model for these glasses is presented.

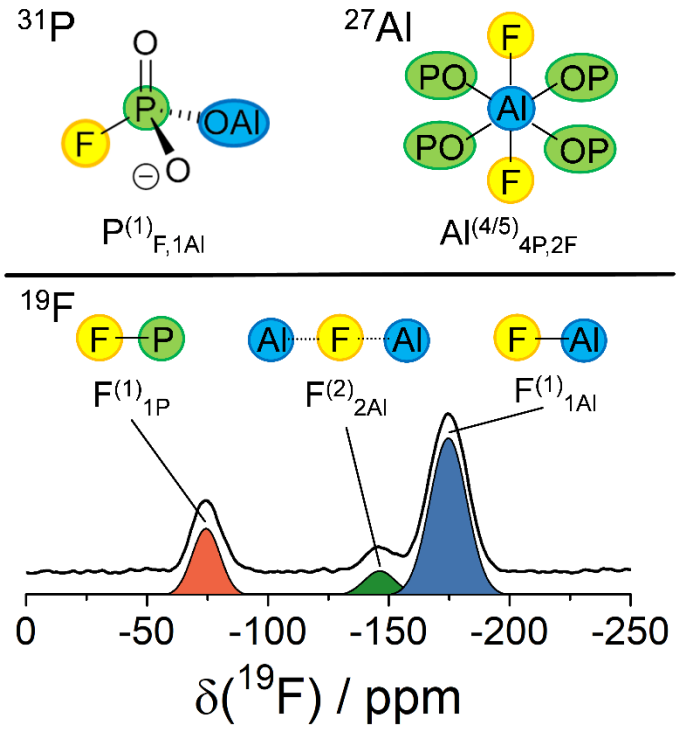

1. INTRODUCTION

The introduction of fluorine into oxide glasses leads to changes of the glasses' structure and properties. This has many practical applications, even though the structural details are not yet fully understood. Fluoride phosphate glasses are of special interest as hosts for luminescent rare-earth ions. They combine the favorable optical properties of fluoride glasses with the higher mechanical and thermal stability of phosphate glasses. Aluminum containing fluoride phosphate glasses[1-10] have attracted considerable attention as matrices for rare-earth dopants for active lasers, amplifier glasses and for photoluminescence in the visible region.[11-17] In addition, nanoparticle-containing systems,[18] inorganic-organic hybrid systems[19] and biomaterials are being studied.[20] The goal of tailoring the particular properties of these attractive glasses requires a comprehensive understanding of their structural organization. Raman/IR and NMR studies published recently focus on glasses having rather complex compositions.[21-29] For those glasses, vibrational band assignments remain ambiguous as there is overlap from bands attributable to phosphorus and aluminum polyhedra in different coordination states.[21,22,24,25,27,29] ^{27}Al NMR chemical shifts can differentiate between fluoride and phosphate ligands, but not in a quantitative manner. Finally, ^{31}P chemical shifts are unable to differentiate between phosphorus-fluorine and phosphorus-oxygen bonding.[30]

These interpretational difficulties have resulted in a number of conflicting suggestions concerning the structure of fluoride aluminophosphate glasses.[21,23-25,27,28] For example, Gan[23] and Videau[22] proposed the formation of [AlF_4] units crosslinking between polyphosphate chains. Other authors believe that F is predominantly attached to $Al^{(6)}$ units.[10,21,24,25,27,28] Based on x-ray photoelectron spectroscopic data Brow et al.[24] propose that F preferentially forms F-Al bonds until each Al site is bound to a maximum of three F atoms. According to these authors, fluoride incorporation beyond this limit proceeds via the formation of F-P bonds.

Solid-state nuclear magnetic resonance (NMR) techniques belong to the most powerful characterization tools for disordered materials. They are element-selective, inherently quantitative, and can provide a wealth of local structural information.[31] In particular, advanced techniques such as rotational echo double resonance (REDOR),[32-34] which utilize through-space internuclear dipole-dipole coupling have provided quantitative information on structural connectivity and spatial proximity in and beyond the first coordination sphere in glasses. Recently we have used these techniques, for the first time, to investigate the structure of rare-earth doped fluoride phosphate

glasses with rather complex compositions. Specifically, we could obtain useful structural insights into the systems $50MF_2$-$(30-x)Al(PO_3)_3$-$xAlF_3$-$(20-z)M'F_3$:$zREF_3$. (M = BaF_2/SrF_2, x = 25, 20, and 15, M' = Sc, Y, and RE = Yb and Eu and $0 \leq z \leq 1.0$).[14,16,35-37] Nevertheless, the interpretation of the NMR data in terms of structure is somewhat tentative owing to the compositional complexity of the materials. Thus, for testing the ability of advanced solid-state NMR methods give information on network structure, it is desirable to study some compositionally simple standards. $(NaPO_3)_{1-x}(AlF_3)_x$ glasses are a useful model system in this regard. They can be prepared over the composition range $0 \leq x \leq 0.4$, and a comprehensive characterization of their macroscopic properties has already been published.[28] The glasses host four useful nuclear probes, ^{19}F, ^{23}Na, ^{27}Al, and ^{31}P, which can be used to characterize local environments and spatial correlations between selected sets of nuclei based on magnetic dipole-dipole interactions. Altogether this glass system presents the opportunity of studying five different heteronuclear distance correlations (Na-F, Na-P, P-F, Al-F, P-Al) by ten distinct double resonance experiments, involving all of the constituent elements present. Based on these experiments and their detailed compositional dependence we develop a detailed structural description of this glass system.

2. EXPERIMENTAL SECTION

2.1 Preparation and Characterization of the glasses

Glass samples with batch compositions $(NaPO_3)_{1-x}(AlF_3)_x$ (x = 0.0, 0.2, 0.3, and 0.4) were prepared by standard melt-cooling. The raw materials were powdered optical grade $NaPO_3$, AlF_3, and NH_4HF_2. The F-free $NaPO_3$ glass was melted in an open amorphous silica crucible at 800°C for 1 h. Glass samples containing AlF_3 were prepared in Pt crucibles with additional 5 wt. % NH_4HF_2 as a fluorinating agent. We applied a 3-step melting procedure: i) 30 min at 400°C, ii) 30 min at 800°C, and iii) 15 min at 850°C. The raw material AlF_3 has a significant problem with variable water and flourine content, as hydroxyl ions (OH^-) can substitute fluorine ions (F^-) in the crystal structure. For a reliable synthesis, NH_4HF_2 was added to fluorinate the raw material AlF_3 by decomposition into NH_3 and HF at lower temperature. In addition NH_4HF_2 ensures an HF-rich, oxygen-depleted atmosphere above the melt and suppresses the often observed F->O exchange reaction between the melt and water from the atmosphere. All melts were poured into preheated graphite molds and cooled from T_g + 50 K to room temperature with a cooling rate of 3-5 K/min. Glass samples obtained had good optical quality; selected properties are given in Table 1. The

refractive indices n_e were measured in the visible range with a Pulfrich refractometer to an accuracy of ± 0.00005, and the dispersion coefficients v_e were determined. The n_e-values decrease and the v_e-values increase with increasing AlF_3 content. Optical absorption was recorded from 3200 to 200 nm on polished plates with a commercial spectrometer from SHIMADZU (error < 1%). The UV absorption edge for all glass samples was below 200 nm on samples with 1 mm thickness. The OH content was determined from the absorption band around 3200 nm (O-H – stretching mode) (see Supporting Materials).[38] The $NaPO_3$ glass sample had a very high OH content, with $(E/d)_{3100nm}$ = 30 cm^{-1}, corresponding to 900 ppmw OH. With introduction of AlF_3 the OH content decreases drastically to 2.8 cm^{-1} ≈ 84 ppmw and 0.3 cm^{-1} ≈ 9 ppmw, as the chemical stability of the glasses increases. The glass transition temperature T_g and the coefficient of thermal expansion (*CTE*) were determined by dilatometry using a heating rate of 5 K/min. The T_g-values increase and the *CTE*-values decrease with increasing AlF_3 content. The density values, measured by the Archimedes method in CCl_4 within ± 0.001 gcm^{-3} increase with increasing AlF_3-content. The fluorine content of the glass samples was analyzed by wet chemical analysis with a precision of ± 0.01 wt%, following the method of Pietzka und Ehrlich[39] (The sample is boiled in H_3PO_4 after addition of SiO_2 powder. The gaseous SiF_4 produced is collected in NaOH solution, resulting in a solution of F^- ions. The latter are precipitated as PbBrF which, through the addition of $AgNO_3$, can be transformed into AgBr. The amount of AgBr is determined titrimetically through re-titration of $Na_2S_2O_3$ against SCN^-). The deviation from the theoretical fluorine content was below 15 %.

Table 1: Glass samples and properties

Sample in mol%	[F] / wt% theor.	[F] / wt% anal.	T_g / °C	*CTE* / $ppmK^{-1}$	Refractive Index, n_e	Dispersion coeff., v_e	Density / gcm^{-3}	[OH] / ppmw
$100NaPO_3$	-	-	260	24.5	1.4858	65	2.52	900
$80NaPO_3$-$20AlF_3$	11.6	10.0	305	21.5	1.4722	71	2.63	84
$70NaPO_3$-$30AlF_3$	17.7	15.6	335	19.0	1.4689	73	2.71	9
$60NaPO_3$-$40AlF_3$[a]	24.1	24.0	405	n.d.[b]	1.4344	80	n.d.[b]	n.d.[b]

[a]sample containing a few $AlPO_4$ crystals, [b]n.d. = not determined

2.2 NMR Studies

Single resonance MAS NMR spectra were recorded at 5.7, 11.7, and 14.1 T on an Agilent spectrometer interfaced to a 5.7 T magnet, a Bruker DSX-500 spectrometer and a Bruker Avance

Neo 600 MHz spectrometer. ^{23}Na, ^{27}Al and ^{31}P high-resolution solid-state NMR measurements were conducted at resonance frequencies of 159, 156 and 243 MHz respectively with a commercial 2.5 mm MAS-NMR probe and a MAS rotation frequency of 15.0 kHz. In addition, double quantum filtered ^{31}P MAS NMR spectra were obtained, with a 1D refocused INADEQUATE experiment[40,41] under identical conditions as the MAS experiments but with a threefold increased number of scans. Phosphorus species involved in P-O-P linkages were selectively detected while signals from other species were suppressed by appropriate phase cycling. Spinning rates and pulse lengths were identical to those chosen for the MAS experiments and double quantum coherence was created during a mixing time of 16.6 ms corresponding to a $^{2}J(^{31}\text{P}\text{-}^{31}\text{P})$ coupling constant of 30 Hz. ^{19}F high-resolution solid-state NMR measurements were done at a resonance frequency of 228 MHz with a 3.2 mm MAS NMR probe at a MAS rotation frequency of 25.0 kHz. Typical employed excitation pulse widths for single-pulse measurements were 1.7 μs (90° flip angle) for ^{31}P, 1.0 μs (30° flip angle) for ^{27}Al and ^{23}Na and 2.0 μs (90° flip angle) for ^{19}F. Recycle delays of 350 and 10 s were used for ^{31}P and ^{19}F and 1 s for ^{27}Al and ^{23}Na experiments, respectively. Chemical shifts are reported relative to aqueous solutions of 1 M $Al(NO_3)_3$, 1 M NaCl, 85 % H_3PO_4 and liquid $CFCl_3$, respectively.

^{27}Al{^{31}P} and ^{31}P{^{23}Na} REDOR experiments were carried out on a Bruker DSX-400 spectrometer operating at 9.4 T, using a 4 mm Bruker triple resonance probe at spinning frequencies of 10.0 – 15.0 kHz. ^{23}Na{^{31}P} REDOR and single-point ^{31}P{^{27}Al} REAPDOR experiments were performed on a Bruker Avance Neo 600 MHz spectrometer, using a commercial 2.5 mm triple resonance probe and a spinning rate of 15.0 and 20.0 kHz respectively. Single-point ^{31}P{^{19}F} REDOR experiments were conducted on a 5.7 T Agilent spectrometer, in a commercial 3.2 mm triple resonance probe at 20.0 kHz MAS frequency. All the other REDOR experiments involving ^{19}F nuclei utilized a 2.5 mm Bruker X-^{19}F/^{1}H double resonance probe in a Bruker DSX-500 spectrometer at spinning frequencies within the range of 15.0-35.0 kHz. The specific methodology used is described in the Supporting Materials Section, and the pulse sequences used are displayed in Figure S1. Table S1 (Supporting Materials Section) summarizes the specific conditions used in the present study. All the $S\{I=1/2\}$ REDOR experiments were measured with the pulse sequence of Figure S1a. In the ^{27}Al{^{31}P} REDOR measurements, a compensation scheme described in Ref. 42 was used to correct for the effect of experimental pulse-imperfections. ^{31}P{^{23}Na} and ^{19}F{^{23}Na}

REDOR measurements were conducted with the pulse sequence of Figure S1b. The π-pulses applied to the spin-1/2 nuclei were phase cycled according to the XY-4 scheme.[32]

3. RESULTS AND DISCUSSION

3.1. ^{23}Na, ^{19}F, and ^{27}Al MAS NMR. Figure 1 (left) shows the ^{23}Na MAS NMR spectra of vitreous $NaPO_3$ and $NaPO_3$-AlF_3 glasses, and further ^{19}F (center), and ^{27}Al (right) MAS NMR spectra of the latter. Table 2 and 3 summarize the multinuclear NMR lineshape parameters of the glasses under study and vitreous $NaPO_3$.

The ^{27}Al MAS NMR spectra show that the current glasses have significantly higher $Al^{(6)}$ contents than F-free aluminum oxide glasses with identical P/Al ratios. This result confirms the fluorine induced enhancement of $Al^{(6)}$ fraction noticed previously in sol-gel prepared fluoride glasses.[43] Six-coordinated aluminum species are predominant in NAPF-20 and NAPF-40 while only small amounts (≤ 8% in NAPF-40) of $Al^{(5)}$ and traces of $Al^{(4)}$ (≤ 1% in NAPF-40) are detectable.

The ^{19}F-NMR spectra allow a quantitative discrimination of three distinct types of fluorine species at chemical shifts near -76, -147 and -176 ppm. The signal at -76 ppm can be assigned to fluorine species bonded to phosphorus ("*fluorophosphate*"), $F^{(1)}{}_{1P}$. The signal near -147 ppm indicates fluorine species bridging two octahedral Al atoms, $F^{(2)}{}_{2Al}$ units, and the dominant signal near -176 ppm represents terminal Al-bonded fluorine species, $F^{(1)}{}_{1Al}$.[43] Within the limits of experimental error, the concentrations of $F^{(1)}{}_{1P}$ units do not depend on composition. In contrast, the concentrations of the Al-bonded fluoride species (both bridging and non-bridging) increase proportionally to AlF_3 content.

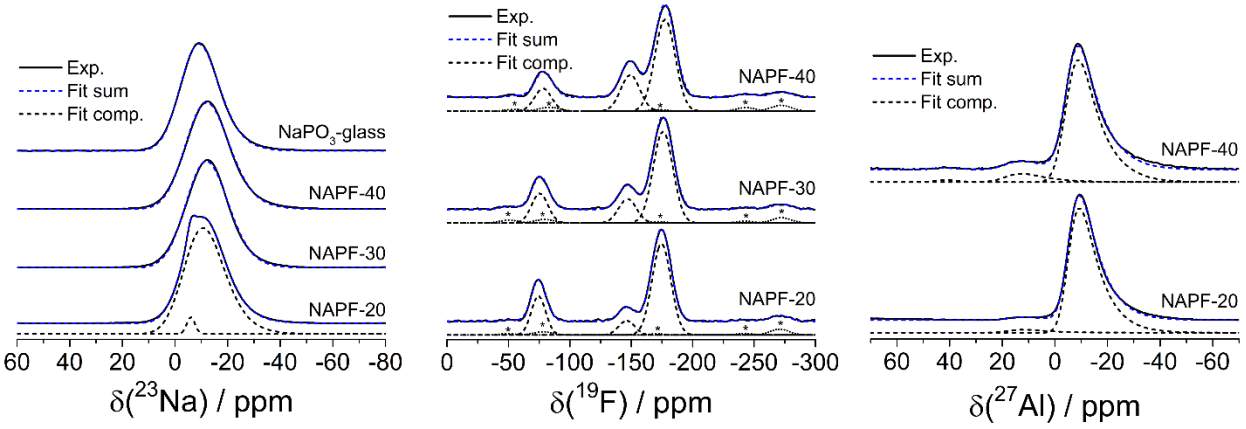

Figure 1: ^{23}Na (left), ^{19}F (center) and ^{27}Al (right) MAS NMR spectra of $NaPO_3$-AlF_3 glasses and glassy $NaPO_3$. Spinning sidebands are indicated by asterisks.

Table 2: ^{19}F MAS NMR parameters for the $NaPO_3$-AlF_3 glasses. Errors for the parameters δ_{CS}^{iso}, *FWHM*, and area fractions are ± 0.3 ppm, ± 0.1 MHz, ± 3%.

Sample	δ_{CS}^{iso} (^{19}F) / ppm			*FWHM* / ppm			MAS Area fractions *f* / %		
	$F^{(1)}_{1P}$	$F^{(2)}_{2Al}$	$F^{(1)}_{1Al}$	$F^{(1)}_{1P}$	$F^{(2)}_{2Al}$	$F^{(1)}_{1Al}$	$F^{(1)}_{1P}$	$F^{(2)}_{2Al}$	$F^{(1)}_{1Al}$
$80NaPO_3$-$20AlF_3$	-75.5	-147.0	-176.0	15.7	17.2	19.0	23	10	67
$70NaPO_3$-$30AlF_3$	-76.1	-147.5	-176.8	15.9	17.5	19.2	18	18	64
$60NaPO_3$-$40AlF_3$	-78.1	-149.2	-177.5	16.3	18.4	19.4	14	24	62

Table 3: ^{23}Na (top) and ^{27}Al (bottom) simulation parameters used in the applied Czjzek model[44] for spectral deconvolutions in $NaPO_3$-AlF_3 glasses.

Sample	^{23}Na MAS NMR		
	δ_{CS}^{iso} (^{23}Na) / ppm	C_Q / MHz	Area fractions *f* / %
$NaPO_3$ glass	-4.2	2.3	100
$80NaPO_3$-$20AlF_3$	-5.3	2.4	97
impurity	-6.0	-	3
$70NaPO_3$-$30AlF_3$	-6.8	2.3	100
$60NaPO_3$-$40AlF_3$	-7.3	2.2	100
Sample / species	^{27}Al MAS NMR		
	δ_{CS}^{iso} (^{27}Al) / ppm	C_Q / MHz	Area fractions *f* / %
$80NaPO_3$-$20AlF_3$			
$Al^{(6)}$	-4.8	5.3	97
$Al^{(5)}$	17.5	5.7	3
$60NaPO_3$-$40AlF_3$			
$Al^{(6)}$	-4.5	5.1	91
$Al^{(5)}$	19.0	6.0	8
$Al^{(4)}$	44	3.3	1

3.2. ^{31}P Single- and double resonance MAS NMR.

Figure 2 shows the ^{31}P NMR MAS-NMR spectra. They show poorly resolved resonance lines with their center of gravity near -19 ppm, which provide little structural information. As indicated in this figure, the double-quantum filtered spectra look very similar and offer no opportunities for spectral editing in this case. The same is true for the ^{31}P{^{19}F} and ^{31}P{^{27}Al} REDOR experiments in the case of the glass containing 40 mole% AlF_3 (see Figure S2, Supporting Materials Section). In the case of the glass containing 20 mole% AlF_3 some distinct differences can be seen between the ^{27}Al dipolar recoupled spectra (S) and the REDOR difference spectra $\Delta S = S_0$-S, which allow the straightforward identification and definition of lineshape parameters for the $P^{(2)}_{0Al}$ units, which are more remote from both Al and F species. From these experiments and analyses we may conclude that the large majority of the P species present in these glasses still contain P-O-P linkages and are in spatial proximity to F and Al. As illustrated in Figure 2 the lineshapes can be simulated with five principal Gaussian deconvolution components, whose parameters are summarized in Table 4. While there are obviously many other possibilities of fitting these poorly resolved lineshapes, the fitting model suggested here takes into consideration previous results on fluoride-free sodium aluminophosphate glasses,[45] and the compositional evolution of the various lineshape components. For example, the fractional areas of these five components show the expected monotonic dependence on AlF_3 content, further confirming the assignments. As discussed previously[45] these signals reflect overlapping $Q^{(n)}_{m\mathrm{Al}}$ species, having variable numbers of P-O-P and Al-O-P linkages n and m. Figure 3 depicts and labels these units, in both the $Q^{(n)}_m$ and the $P^{(n)}_m$ terminology. In the $Q^{(n)}_{m\mathrm{Al}}$ terminology, the superscript n denotes the number of P-O-P linkages, whereas in the $P^{(n)}_{m\mathrm{Al}}$ terminology the superscript n denotes the number of bridging oxygen atoms, counting all oxygen atoms linking to aluminum atoms as bridging ones.

The ^{31}P{^{19}F} REDOR difference spectra recorded at a short dipolar mixing time (4 rotor cycles, see Figure S2, Supporting Materials Section) are dominated by the F-bonded phosphate species $Q^{(0)}_{F,1Al}$ (= $P^{(1)}_{F,1Al}$), $Q^{(1)}_{F,0Al}$ (= $P^{(1)}_{F,0Al}$) and $Q^{(1)}_{F,1Al}$ (= $P^{(2)}_{F,1Al}$) units (Figure 3b). Their signals contribute to the deconvolution components attributed to the $Q^{(1)}_{0Al}$ ($P^{(1)}_{0Al}$) and $Q^{(0)}_{1Al}$ ($P^{(1)}_{1Al}$) (both near -11 ppm) and the $Q^{(1)}_{1Al}$ ($P^{(2)}_{1Al}$) units (near -15 ppm), respectively. In principle there may also be F-bearing species with higher connectivities (such as $Q^{(2)}_{F,1Al}$ (= $P^{(3)}_{F,1Al}$) units, which would contribute intensity to signal components at lower frequencies.

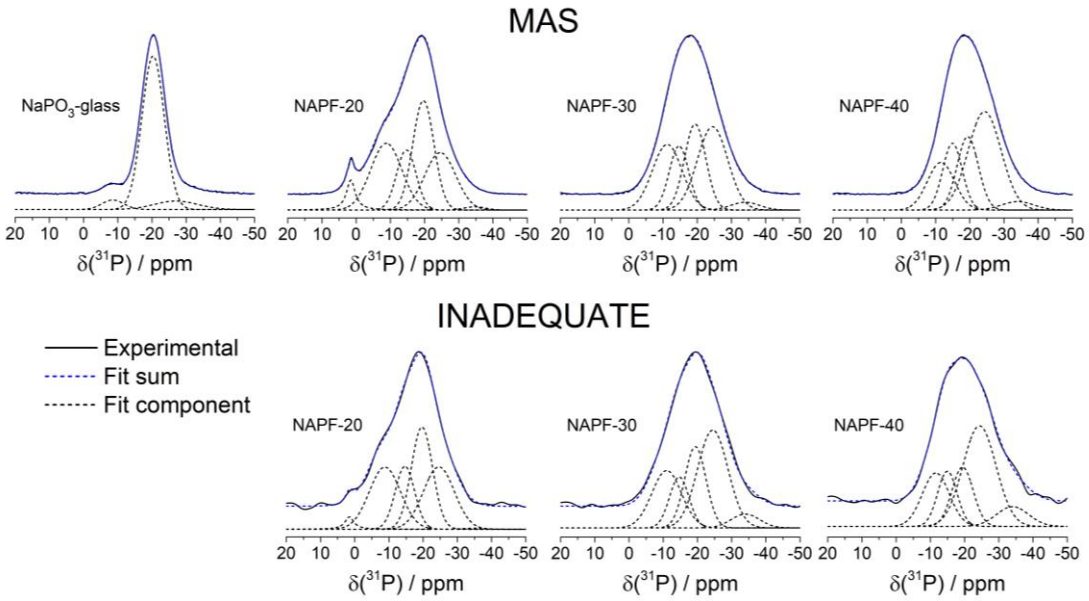

Figure 2: ^{31}P MAS NMR and INADEQUATE spectra of the studied glasses and of pure $NaPO_3$ glass.

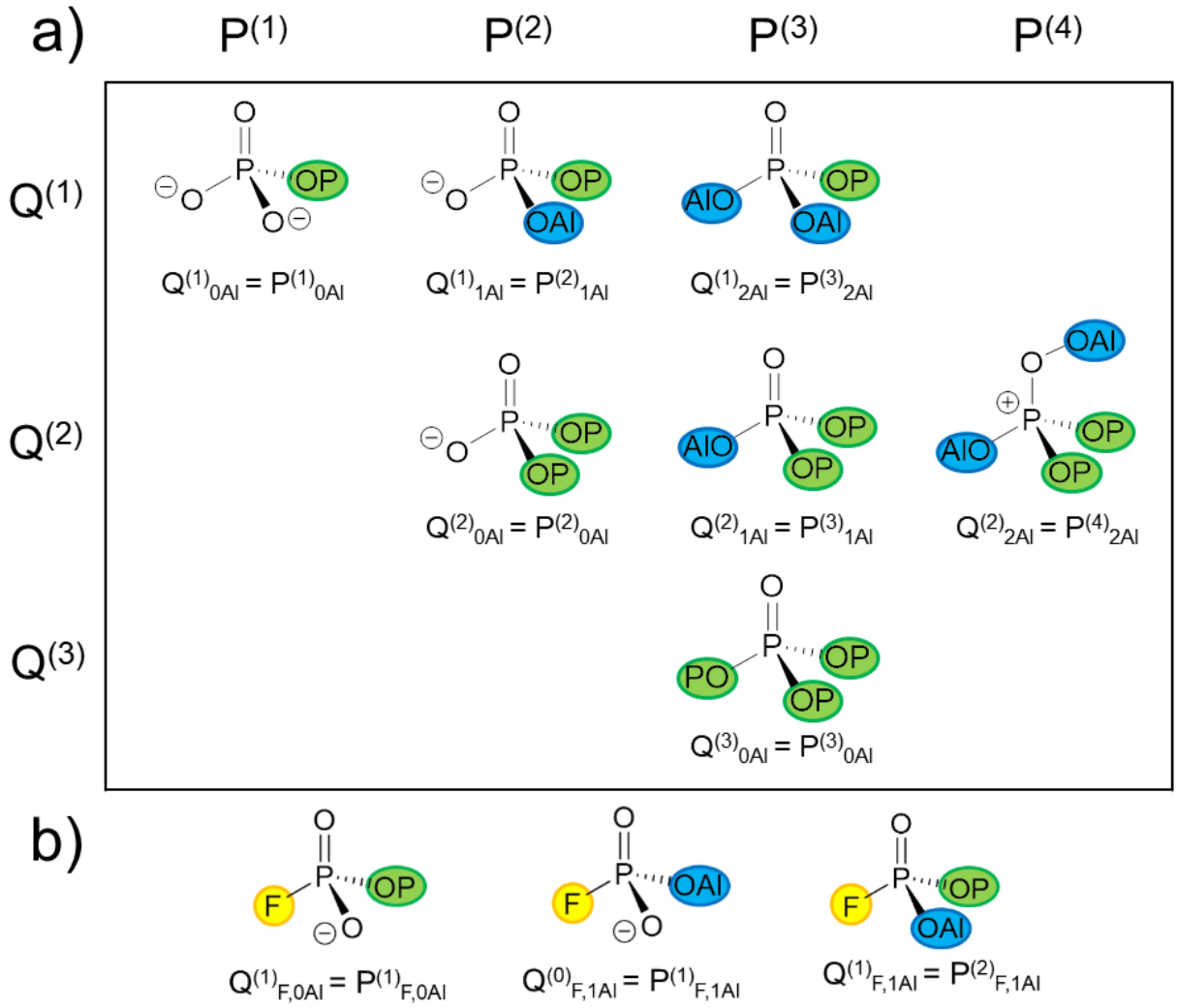

Figure 3: Network forming units inferred to be present in $NaPO_3$-AlF_3 glasses. a) phosphate units, b):fluorophosphate units.

Table 4: ^{31}P MAS and INADEQUATE NMR deconvolution parameters δ_{CS}^{iso} (chemical shift) and *FWHM* (full width at half maximum) for the $NaPO_3$-AlF_3 glasses. Reported area fractions from MAS NMR take into account spinning sideband intensities. MAS and INADEQUATE spectra were deconvoluted with purely Gaussian components, in which sample-to-sample variations of parameters were kept at a minimum.

Sample in mol% / Component	δ_{CS}^{iso} (^{31}P) / ppm	*FWHM* / ppm	MAS Area fractions *f* / %
$NaPO_3$ (glass)			
$Q^{(1)}_{0Al} = P^{(1)}_{0Al}$	-9.0	7.5	4
$Q^{(2)}_{0Al} = P^{(2)}_{0Al}$	-20.3	7.7	87
$Q^{(3)}_{0Al} = P^{(3)}_{0Al}$	-27.0	14.8	9
$80NaPO_3$-$20AlF_3$			
$P_2O_7^{2-}$-group[a]	1.6	3.0	3
$Q^{(1)}_{0Al} = P^{(1)}_{0Al}$	-8.8	10.7	22[b]
$Q^{(1)}_{1Al} = P^{(2)}_{1Al}$	-14.7	6.7	14[c]
$Q^{(2)}_{0Al} = P^{(2)}_{0Al}$	-19.7	7.3	35
$Q^{(2)}_{1Al} = P^{(3)}_{1Al}$	-24.6	10.7	25
$Q^{(2)}_{2Al} = P^{(4)}_{2Al}$	-34.6	7.3	1
$70NaPO_3$-$30AlF_3$			
$Q^{(1)}_{0Al} = P^{(1)}_{0Al}$	-11.2	10.2	25[b]
$Q^{(1)}_{1Al} = P^{(2)}_{1Al}$	-14.7	6.7	14[c]
$Q^{(2)}_{0Al} = P^{(2)}_{0Al}$	-19.7	7.3	24
$Q^{(2)}_{1Al} = P^{(3)}_{1Al}$	-24.5	10.4	34
$Q^{(2)}_{2Al} = P^{(4)}_{2Al}$	-34.0	9.8	3
$60NaPO_3$-$40AlF_3$			
$Q^{(1)}_{0Al} = P^{(1)}_{0Al}$	-11.6	9.3	18[b]
$Q^{(1)}_{1Al} = P^{(2)}_{1Al}$	-15.0	6.7	16[c]
$Q^{(2)}_{0Al} = P^{(2)}_{0Al}$	-19.4	7.3	20
$Q^{(2)}_{1Al} = P^{(3)}_{1Al}$	-24.3	11.4	42
$Q^{(2)}_{2Al} = P^{(4)}_{2Al}$	-34.0	11.0	4

[a] Purely Lorentzian line shape, [b]includes contributions from $Q^{(0)}_{F,1Al}$ (= $P^{(1)}_{F,1Al}$) and $Q^{(1)}_{F,0Al}$ (= $P^{(1)}_{F,0Al}$) units, [c]includes contributions from $Q^{(1)}_{F,1Al}$ (= $P^{(2)}_{F,1Al}$) units.

Figure 4 depicts $^{31}P\{^{23}Na\}$ REDOR dephasing curves for the glasses with 20 and 30 percent AlF_3 as well as pure vitreous $NaPO_3$ and crystalline Na_2PO_3F. While the $M_{2(P\text{-}Na)}$ value for Na_2PO_3F

matches the van Vleck prediction[46] from the crystal structure within 20 %, (see Table 5), the glasses show significantly lower values in agreement with their lower Na/P ratios. Within the limits of experimental error, the $M_{2(P\text{-}Na)}$ values remain approximately constant for these three glasses. This finding is consistent with the constant Na/P ratio of these glasses.

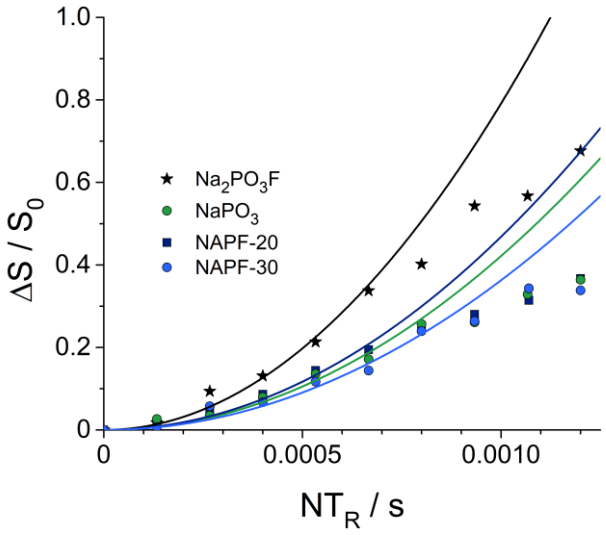

Figure 4: $^{31}P\{^{23}Na\}$ REDOR dephasing curves of $NaPO_3$-AlF_3 glasses, vitreous $NaPO_3$ and the model compound Na_2PO_3F.

Table 5: $M_{2(P\text{-}Na)}$ values obtained from $^{31}P\{^{23}Na\}$ REDOR data. Values in parentheses are as obtained from the parabolic fits to equ. 2 given in the Supporting Materials Section. The other values are corrected ones accounting for the deviation between the model compound's theoretical and experimental M_2 value (factor 0.83)

Sample	**$^{31}P\{^{23}Na\}$ REDOR**	
	$M_{2(P\text{-}Na)}$ / $10^6 rad^2/s^2$ ± 10%	f_1[b]
Na_2PO_3F	(41.4) / 49.7[a]	0.0462
$NaPO_3$	(19.6) / 23.6[a]	0.0656
$80NaPO_3$-$20AlF_3$	(21.8) / 26.3	0.0656
$70NaPO_3$-$30AlF_3$	(17.1) / 20.6	0.0637
$60NaPO_3$-$40AlF_3$	n.d.	n.d.

[a] calculated average van-Vleck second moment[46] over all sites in the crystalline structure.[47-49]
[b] efficiency factor[50] obtained by SIMPSON[51] simulations.

$^{27}Al\{^{19}F\}$ and $^{27}Al\{^{31}P\}$ REDOR. Figure 5 (left) shows the $^{27}Al\{^{19}F\}$ REDOR dephasing curves of the three aluminum containing glasses, as well as for AlF_3 and the obtained $M_{2(Al\text{-}F)}$ values

are listed in Table 6. The experimental $M_{2(Al\text{-}F)}$ -value of 659 × 10^6rad^2/s^2 measured for AlF_3 is significantly lower than the value of 1282 × 10^6rad^2/s^2 expected from the crystal structure.[52] We attribute this large deviation to the steepness of the REDOR curve, which limits the accuracy and precision with which the parabolic fit can be applied. For this reason, we will not rely on the absolute M_2-values measured on our glasses, but rather calibrate them against the experimental results obtained on AlF_3. Within the limits of experimental error, the ^{19}F-^{27}Al magnetic dipole-dipole coupling strength in the three glasses is identical, and significantly lower than in AlF_3. This result indicates that the number of Al-F bonds in these glasses is approximately constant and not strongly dependent on composition.

Figure 5 (right) shows the ^{27}Al{^{31}P} REDOR measurements of the $NaPO_3$-AlF_3 glasses, indicating an expected significantly weaker ^{31}P-^{27}Al magnetic dipole-dipole coupling compared to fluoride-free $NaPO_3$-Al_2O_3 glasses. In the latter system, the size of the measured ^{27}Al-^{31}P dipolar coupling corresponds to six Al-O-P linkages, which in turn allows a quantification of the average number of Al-O-P bonds (CN_{AlOP}) and Al-F bonds ($CN_{Al\text{-}F}$) per Al$^{(6)}$ unit in the F-containing glasses via the following expressions:

$$CN_{AlOP} = 6 \times M_{2(Al\text{-}P)} / 6.4 \times 10^6 \text{rad}^2/\text{s}^2 \qquad (4)$$

$$CN_{Al\text{-}F} = 6 \times M_{2(Al\text{-}F)} / 659 \times 10^6 \text{rad}^2/\text{s}^2 \qquad (5)$$

Here, the denominators represent the experimental $M_{2(Al\text{-}P)}$ and $M_{2(Al\text{-}F)}$ for pure $Al(OP)_6$ and AlF_6 environments, as measured on $Al(PO_3)_3$ (theoretically expected $M_{2(Al\text{-}P)}$: 7.8 ×10^6rad^{2}s^{-2})[53] and AlF_3. Equations (4) and (5) imply that these M_2 values scale linearly with the number of Al-O-P or Al-F linkages, which holds provided no large variations in the corresponding internuclear distances occur. Table 6 summarizes the calculated average numbers of phosphorus (CN_{AlOP}) and fluorine ($CN_{Al\text{-}F}$) bonded to Al$^{(6)}$ units. The sum of CN_{AlOP} and $CN_{Al\text{-}F}$ turns out to be close to 6 for the two glasses with 20 and 30 mole% AlF_3. The somewhat larger deviation observed for the glass with 40 mole% AlF_3 is still within the experimental error limits and comparable to similar results obtained by us in analogous analyses of other fluoride-phosphate glasses.[43] Based on these numbers, the average coordination of Al$^{(6)}$ in these glasses can be described approximately by an $Al(OP)_4F_2$ environment. As an independent check on these results we can estimate the F/Al ratio in these glasses from the expression.

$$[F]/[Al] = CN_{Al\text{-}F}/CN_{F\text{-}Al} + 3 \times f(F^{(1)}{}_{1P}) \qquad (6)$$

where the first term refers to the Al-bound F and the second term to the P-bound F species.

In eq. (6) $CN_{Al\text{-}F}$ is the average number of F ligands per $Al^{(6)}$ unit as determined from REDOR and $CN_{F\text{-}Al}$ is the average number of F-Al bonds for fluorine, calculated by

$$CN_{F\text{-}Al} = 2\times f(F^{(2)}{}_{2Al}) + 1\times f(F^{(1)}{}_{1Al})/\ \{f(F^{(2)}{}_{2Al}) + f(F^{(1)}{}_{1Al})\} \quad (7)$$

where $f(F^{(2)}{}_{2Al})$ and $f(F^{(1)}{}_{1Al})$ represent the relative concentrations of bridging and terminating fluorine atoms, obtained from Table 2. As Table 6 indicates, the calculated F/Al ratios are generally found somewhat lower than 3:1. This result is understandable considering the fluorine loss indicated by the analytical data. Thus, overall consistent results are obtained, suggesting the validity of the quantitative approach outlined above.

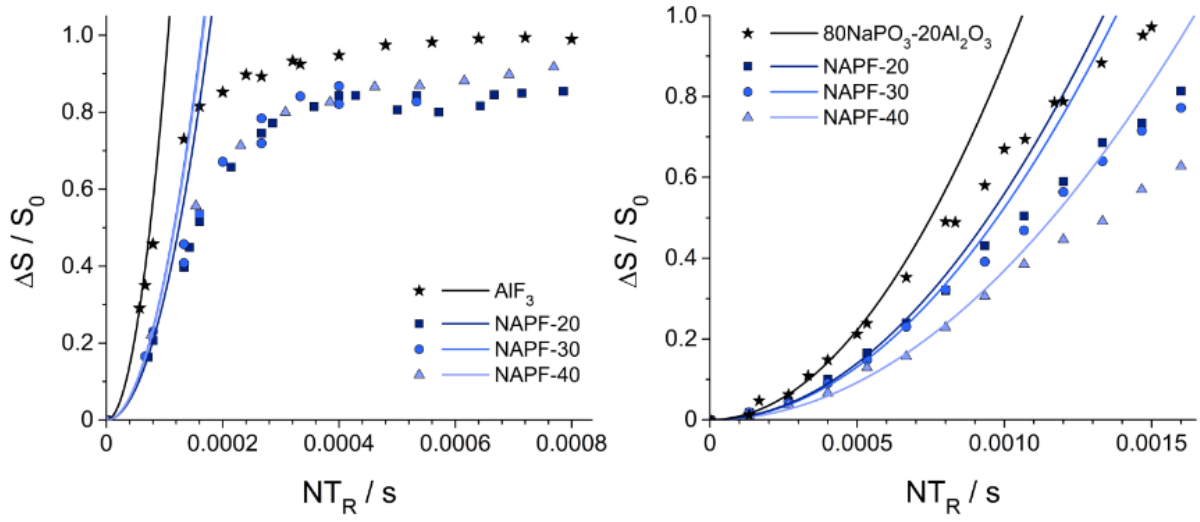

Figure 5: $^{27}Al\{^{19}F\}$ REDOR (left) and $^{27}Al\{^{31}P\}$ REDOR (right) dephasing curves of $NaPO_3$-AlF_3 glasses, and model compounds: crystalline AlF_3 and a fluoride free glass of comparable composition (80 $NaPO_3$-20Al_2O_3).

Table 6: Second moments (± 10 %) extracted from $^{27}Al\{^{31}P\}$ and $^{27}Al\{^{19}F\}$ REDOR dephasing curves for $Al^{(6)}$, the average coordination numbers and the calculated F/Al ratio deduced from these results. Reported Al-F second moments have been corrected by a factor $F = 0.51$, accounting for the deviation between the model compound's theoretical and experimental M_2 value. Values in parentheses are as obtained from the parabolic fits (see experimental section).

Sample	$^{27}Al\{^{31}P\}$ REDOR		$^{27}Al^{(6)}\{^{19}F\}$ REDOR		[F]/[Al]
	$M_{2(Al\text{-}P)}$ / $10^6 rad^2/s^2$	CN_{AlOP} ± 10%	$M_{2(Al\text{-}F)}$ / $10^6 rad^2/s^2$ ± 10%	$CN_{Al\text{-}F}$	
AlF_3	-	-	(659) / 1282.2 [a]	6	-
80$NaPO_3$-20Al_2O_3	6.4	6.0±0.6	-	-	-
80$NaPO_3$-20AlF_3	4.3	4.0±0.4	(238) / 463	2.1±0.2	2.6±0.4
70$NaPO_3$-30AlF_3	3.9	3.7±0.4	(269) / 523	2.4±0.2	2.5±0.4

$60NaPO_3$-$40AlF_3$	2.9	2.7±0.3	(275) / 538	2.3±0.2	2.6±0.4

[a] calculated average van-Vleck second moment over all sites in the corresponding crystalline structure.[52]

^{19}F{^{31}P} and ^{19}F{^{23}Na} REDOR. Figure 6 (left) depicts the measured ^{19}F{^{31}P} REDOR curves of the $NaPO_3$-AlF_3 glasses and the crystalline model compound Na_2PO_3F. An excellent distinction between P- and Al-bonded fluorine species is expected from this experiment as the dipolar coupling constant of a short F-P linkage is rather strong. Indeed, a strong dipolar dephasing of the P-bonded fluorine species ($F^{(1)}{}_{1P}$, peak near -75 ppm) is observed in both the model compound and the glasses. While these curves do not allow a further distinction here, owing to the comparatively coarse sampling rate of the REDOR curve (limited by the MAS spinning rate), we may conclude that the P-F bond lengths in the glasses are the same, within the experimental error, as that of the model compound. The $M_{2(F\text{-}P)}$ values measured for the two types of Al-bound F species reflect much weaker dipolar interactions (see Table 6). This is expected as the closest F···P approach occurs only within the third coordination sphere via **P**-O-Al$^{(6)}$-**F** fragments. Furthermore, the $F^{(2)}{}_{2Al}$ species show consistently larger $M_{2(F\text{-}P)}$ values compared to the $F^{(1)}{}_{1Al}$ species; this can be explained on the basis of their higher connectivity, promoting third-nearest neighbor interactions with twice the number of P-bonded Al species. Within the glass series studied here, the $M_{2(F\text{-}P)}$ measured for the $F^{(1)}{}_{1Al}$ and $F^{(2)}{}_{2Al}$ species tend to decrease with decreasing P content which is expected owing to the concomitant dilution effect.

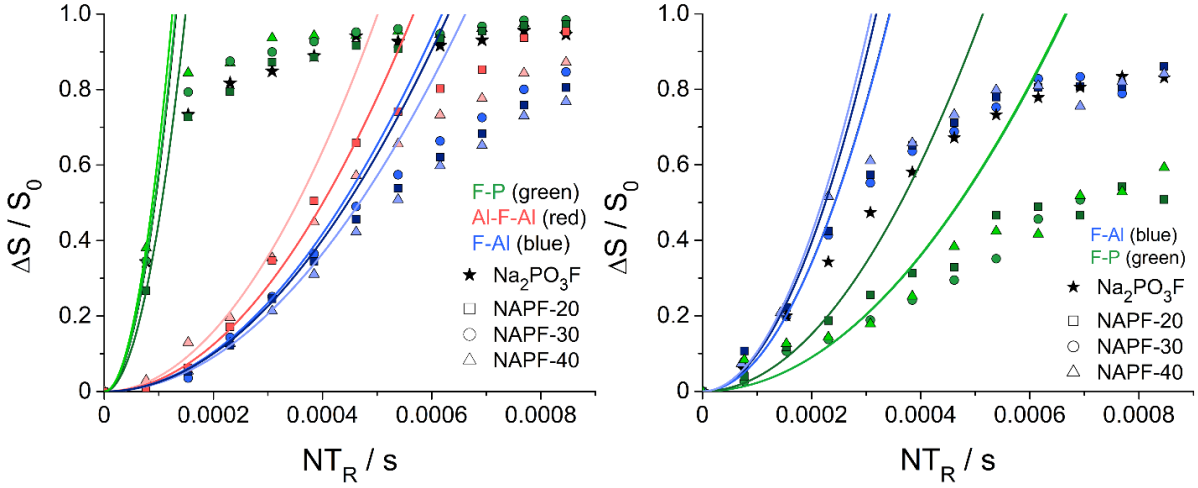

Figure 6: ^{19}F{^{31}P} REDOR (left) and ^{19}F{^{23}Na} REDOR (right) dephasing curves of $NaPO_3$-AlF_3 glasses and Na_2PO_3F.

Figure 6 (right) shows the $^{19}F\{^{23}Na\}$ REDOR results. The data were analyzed according to eq. 2, based on the experimentally found nuclear electric quadrupolar coupling parameters of ^{23}Na (Table 2) and f_1 values, which are listed together with the resulting $M_{2(F\text{-}Na)}$ values in Table 7. For the model compound Na_2PO_3F it was found that the procedure tends to underestimate the dipolar second moment by about 15-20%. The $M_{2(F\text{-}Na)}$ values listed for the glasses are therefore re-calibrated accordingly. Note that in the glasses, the Al-bound terminal fluoride species $F^{(1)}{}_{1Al}$ interact much more strongly with sodium than the P-bound fluoride species, $F^{(1)}{}_{1P}$. This preference is not unexpected as six-coordinate Al species connected to bridging oxygen and terminal fluoride species are formally anionic, resulting in strong Coulombic attractive forces towards the cations. For the $F^{(1)}{}_{1P}$ species, the ^{19}F nuclei experience a significantly weaker dipolar field than in the model compound Na_2PO_3F. This is also expected, as the Na/F ratio in the glasses is lower than in the model compound. Consistent with this dilution effect, $M_{2(F\text{-}Na)}$ tends to decrease with increasing AlF_3 content for both types of F species.

Table 7: The second moments extracted from $^{19}F\{^{31}P\}$ and $^{19}F\{^{23}Na\}$ REDOR curves. Typical errors for the M_2-values are less than ±10% unless indicated otherwise. Reported F-P and F-Na second moments have been corrected by a factor $F = 0.44$ and $F = 0.81$ respectively, accounting for the deviation between the model compound's theoretical and experimental M_2 value. Values in parentheses are as obtained from the parabolic fits (see experimental section).

Sample	**$^{19}F\{^{31}P\}$ REDOR**			**$^{19}F\{^{23}Na\}$ REDOR**		
	M_2 / 10^6rad^2/s^2					f_1[a]
	$F^{(1)}{}_{1P}$	$F^{(2)}{}_{2Al}$	$F^{(1)}{}_{1Al}$	$F^{(1)}{}_{1P}$	$F^{(1)}{}_{1Al}$	
Na_2PO_3F	(430) / 968.9[b]	-	-	(372.0) / 460.7[b]	-	0.077
$80NaPO_3$-$20AlF_3$	(334) / 752[c]	(29.5) / 66.4	(18.6) / 41.9	(134) / 165	(348.0) / 431	0.122
$70NaPO_3$-$30AlF_3$	(433) / 975[c]	(23.1) / 52.0	(19.3) / 43.5	(79) / 98	(300.0) / 372	0.122
$60NaPO_3$-$40AlF_3$	(476.0) / 1072[c]	n.d.	(16.9) / 38.1	(80) / 99	(368.0) 454.3	0.122

[a] efficiency factor[50] obtained by SIMPSON simulations.[51]
[b] calculated average van-Vleck second moment[46] over all sites in the crystalline structure.[47]
[c] estimated error ±20%

$^{23}Na\{^{19}F\}$ and $^{23}Na\{^{31}P\}$ REDOR. Figure 7 (left) summarizes the $^{23}Na\{^{31}P\}$ REDOR curves. The curves are relatively close to each other, and likewise to the REDOR curve of crystalline and glassy $NaPO_3$. This result suggests strong ligation of sodium with phosphate for all these glasses, in a manner comparable to the situation in $NaPO_3$, which has the same P/Na ratio as

present in the glasses. With increasing AlF_3 content a slight decrease of $M_{2(Na\text{-}P)}$ can be noted. This effect can be understood in terms of increasing dilution of the sodium and phosphate inventory. Figure 7 (right) shows the $^{23}Na\{^{19}F\}$ REDOR curves of the three glasses and of crystalline Na_2PO_3F. The $M_{2(Na\text{-}F)}$-values are found to be significantly higher than in the model compound, which is easily explained by the fact that the glasses have higher F/Na ratios than Na_2PO_3F. Within the series of glasses studied, the data show a systematic linear increase of $M_{2(Na\text{-}F)}$ with increasing F/Na ratio (see also figure S5), indicating a systematically increased participation of fluoride ions in the first coordination sphere of sodium as the AlF_3 content of the glasses is increased.

A quantification of the average number of direct F ligands to Na ($CN_{Na\text{-}F}$) from the measured $M_{2(Na\text{-}F)}$ values is not trivial, as the second moment values comprise the combined effect of inverse sixth power of internuclear distance and number of neighbors. Thus, the same numerical value may arise for one short Na-F distance or for multiple neighbors at somewhat longer distances. This is illustrated in Table S3, which summarizes the contributions of all the Na-F distances within the crystal structure to $M_{2(Na\text{-}F)}$ for the four distinct sodium sites in Na_2PO_3F. For Na1 and Na2, the shortest Na-F distances of 230 pm clearly dominates the value of $M_{2(Na\text{-}F)}$, making a contribution of 48×10^6 rad^2s^{-2} (to a total value of 60×10^6 rad^2s^{-2} after including the contributions from more remote ^{19}F nuclei). On the other hand, for the Na4 site there are five Na-F distances ranging from 266 to 331 pm, producing about the same contribution 49×10^6 rad^2s^{-2} to the $M_{2(Na\text{-}F)}$ value. Assuming, for the sake of the argument, that the closest F-Na approach in the glasses corresponds to 230 pm, which is the closest distance in both Na_2PO_3F and NaF and corresponds to a second moment contribution of 60×10^6 rad^2s^{-2} we can estimate the number of F atoms within the first coordination sphere of Na by the relationship

$$CN_{Na\text{-}F} = M_2(^{23}Na\{^{19}F\}) / 60.0 \times 10^6 rad^2/s^2.$$

Based on these assumptions we conclude that the number of nearest Na—F neighbors increases linearly from $CN_{Na\text{-}F} = 1$ to $CN_{Na\text{-}F} = 2$, as the F/Na ratio increases from 0.75 ($x = 0.2$) to 2.0 ($x = 0.4$) within this series.

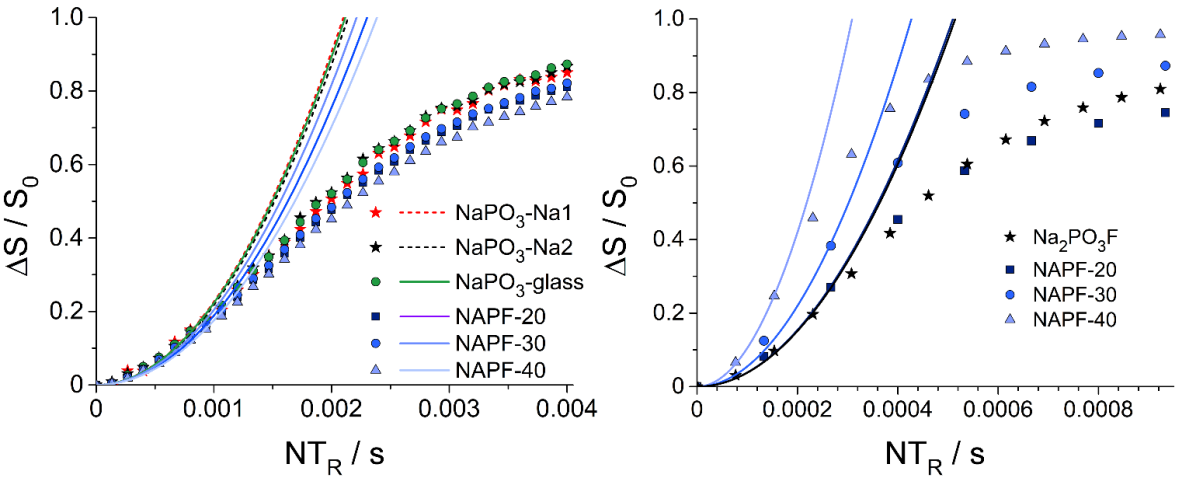

Figure 7: ^{23}Na{^{31}P} REDOR (left) and ^{23}Na{^{19}F} REDOR (right) dephasing curves of pure $NaPO_3$ glass, its isochemical crystal, crystalline Na_2PO_3F and $NaPO_3$-AlF_3 glasses.

Table 8: The second moments extracted from ^{23}Na{^{31}P} and ^{23}Na{^{19}F} REDOR dephasing curves. Reported Na-P and Na-F second moments have been corrected by a factor f = 0.27 and f = 0.60 respectively, accounting for the deviation between the model compound's theoretical and experimental M_2 value. Values in parentheses are as obtained from the parabolic fits (see experimental section).

Sample / site	$M_{2(Na\text{-}P)}$ / 10^6rad^2/s^2 ±10%	$M_{2(Na\text{-}F)}$ / 10^6rad^2/s^2 ±10%	$CN_{Na\text{-}F}$	F / Na
$NaPO_3$ – crystal Na1	(1.68) / 5.7[a]	-		
$NaPO_3$ – crystal Na2	(1.61) / 6.4[a]			
$NaPO_3$ – glass	(1.65) / 6.1	-		
Na_2PO_3F	5.0[b]	(27.6) / 46.1[b]	0.77	0.5
Na1	6.1[b]	60.0[b]	1.0	
Na2	5.5[b]	60.1[b]	1.0	
Na3	3.9[b]	12.6[b]	0.21	
Na4	4.4[b]	50.8[b]	0.85	
80$NaPO_3$-20AlF_3	(1.4) / 5.2	(28.5) / 47.6	0.79	0.75
70$NaPO_3$-30AlF_3	(1.5) / 5.6	(40.6) / 67.8	1.13	1.29
60$NaPO_3$-40AlF_3	(1.3) / 4.8	(77.6) / 129.6	2.16	2.0

[a] calculated van Vleck second moment from crystal structure of $NaPO_3$.[48,49]
[b] calculated individual and average van-Vleck second moment for all four sites in the corresponding crystal structure (see Supporting Materials Section).[47]

4. CONCLUSIONS

All the NMR results summarized above confirm consistently that in $NaPO_3$-AlF_3 glasses the fluorine exists as P-bound, as bridging (Al-F-Al), and as terminal (Al-F) units with the latter being the dominant species owing to the high F/Al ratio of these glasses. Aluminum is predominantly six-coordinated, and the average number of Al-F and Al-O-P linkages can be estimated from combined quantitative $^{27}Al\{^{19}F\}$ and $^{27}Al\{^{31}P\}$ REDOR experiments. In these glasses the local aluminum coordination approaches an $Al(OP)_4F_2$ environment, in which the fluoride species are strongly interacting with the sodium ions. This particular configuration and preferred interaction is characterized by compositionally independent second moment values $M_{2(Al\text{-}F)}$, $M_{2(Al\text{-}P)}$, $M_{2(F\text{-}P)}$ of the P-bound F species, and $M_{2(F\text{-}Na)}$, of the Al-bound F species. In contrast, the compositional trends of the heteronuclear second moment values $M_{2(F\text{-}P)}$ for the Al-bound F species, $M_{2(F\text{-}Na)}$ (for the P-bound F species), $M_{2(Na\text{-}P)}$ and $M_{2(Na\text{-}F)}$ show monotonic dependences on the corresponding atomic ratios involved. These compositional dependences are most consistent with an overall principle of a random relative distribution, causing the M_2 values to be controlled by dilution effects. None of the results presented here give evidence for phase separation effects. Altogether, the present study illustrates the power and potential of multinuclear double resonance NMR experiments for elucidating the structural role of fluoride in sodium aluminophosphate glasses.

A note of caution when comparing $NaPO_3$-AlF_3 glasses with other fluoride phosphate glass systems concerns the P-F bonds, which are unstable at higher temperatures. Depending on the basicity of the cations, P-F bonds break e.g. in $BaPO_3F$ at T>1200°C and in Na_2PO_3F at T>850°C.[54,55] Thus, depending on the glass composition, P-F bonds can be lost when glasses are melted too long at higher temperatures.[14,26,35,36]

ADDITIONAL INFORMATION AVAILABLE

Supporting Materials Section: Description of the REDOR methodology used in the present study, pulse sequences used and experimental conditions; spectral editing experiments using REDOR and REAPDOR, internuclear distance distribution in the model compounds Na_2PO_3F and $NaPO_3$, effect of the chemical shift anisotropy on the REDOR curve of $NaPO_3$.

AUTHOR INFORMATION

*corresponding author, email: eckerth@uni-muenster.de

ACKNOWLEDGEMENTS

Financial support from Deutsche Forschungsgemeinschaft (grants Ec168/3-1 and Ec168/4-2) is gratefully acknowledged. Carla C. de Araujo thanks the NRW Graduate School of Chemistry for a personal stipend, and L. Zhang thanks the DFG (via SFB458) for the support as a visiting scientist to the University of Münster. HE and HB thank FAPESP, process number 07793-6 (CEPID program). D. Möncke thanks FAPESP (process number 2017/029536) for the financial support of a research visit in 2017 at the Laboratório de Materiais Vítreos at the Departamento de Engenharia de Materiais, Universidade Federal de São Carlos, Brazil.

REFERENCES

1. Kuan-Han, S. Fluorophosphate glasses. E. K. Co. USA. US 2511225. (1950).
2.Weber, M. J.; Layne, C. B.; Saroyan, R. A.; Milam, D. (1976). Low-index fluoride glasses for high-power Nd lasers. *Optics Commun*. **1976**, *18*, 171-172.
3. Galant, V. E., Makarenko, N. M.; Petrovskii, G. T.; Urusovskaya, L. N. Thermooptical glasses based on on aluminum metaphosphate and barium fluoride, *Soviet J. Glass Phys. Chem.* **1982** *8*, 404-407.
4. Ehrt, D., Krauß, M.; Erdmann, C.;Vogel, W. (1982). Fluoroaluminatgläser;1) Systeme CaF_2-AlF_3 und MgF_2-CaF_2-AlF_3. *Z. Chem.* **1982**, *22*, 315-316.
5. Ehrt, D.; Vogel, W. Optische Gläser mit anomaler Teildispersion. Feingerätetechnik **1982**, *31* 147-151.
6. Ehrt, D., Erdmann, D.; Vogel, W. Fluoroaluminatgläser; 2. System CaF_2-SrF_2-AlF_3. *Z. Chem*. **1983**, *23*, 37-38.
7. Ehrt, D.;Vogel, W. Fluoroaluminatgläser; 3. Einfluß von Phosphaten auf die Glasbildung im System MgF_2-CaF_2-SrF_2-AlF_3. *Z. Chem*. **1983**, *23***,** 111-112.
8. Djouama, T.,Boutarfaia, A.; Poulain, M. Fluorophosphate glasses containing manganese. *J. Phys. Chem. Solids* **2008**, *69***,** 2756-2763.
9. Nazabal, V., Poulain, M.; Olivier, M.; Pirasteh, P.; Camy, P.; Doualan, J. L.; Guy, S.; Djouama, T.; Boutarfaia, A.; Adam, J. L. Fluoride and oxyfluoride glasses for optical applications. *J. Fluorine Chem*. **2012**, *134* (Suppl. C): 18-23.
10. Ehrt, D. Phosphate and fluoride-phosphate optical glasses - properties, structure and applications. *Phys. Chem. Glasses - Eur. J. Glass Sci. Technol.* Part B **2015**, *56***,** 217-234.
11. Ehrt, D. Structure and properties of fluoride phosphate glasses.*SPIE Proc*. **1992**, *1761*, 213-222.
12. Ehrt, D. Fluoroaluminate glasses for lasers and amplifiers. *Curr. Opinion Solid State & Mater. Sci*. **2003**, *7*, 135-141.
13. Herrmann, A.; Ehrt, D. Green and Red Er^{3+} Photoluminescence behavior in various fluoride glasses. *Int. J.Appl. Glass Sci.* **2010**, *1*, 341-349.
14. Gonçalves, T. S., Moreira Silva, R. J.; de Oliveira Jr, M:, Ferrari, C. R. Poirier, G. Y.; Eckert, H.; de Camargo, A. S. S. Structure-property relations in new fluorophosphate glasses singly- and co-doped with Er^{3+} and Yb^{3+} *Mater. Chem. Phys*. **2015,** *157*, 45-55.
15. Kalnins, C. A. G., Ebendorff-Heidepriem, H.; Spooner, N. A.; Monro, T. M. Enhanced radiation dosimetry of fluoride phosphate glass optical fibres by terbium (III) doping. *Optical Materials Express* **2016,** *6*, 3692-3703
16, Galleani, G., S. H. Santagneli, Y. Messaddeq, M. de Oliveira and H. Eckert (2017). Rare-earth doped fluoride phosphate glasses: structural foundations of their luminescence properties. *Phys. Chem. Chem. Phys* **2017,** *19*, 21612-21624.
17. Galleani, G., Ledemi, Y.; de Lima Filho, E. D.; Morency, S.; Delaizir, G.;. Chenu, S.; Duclere, J. R.; Messaddeq, Y. UV-transmitting step-index fluorophosphate glass fiber fabricated by the crucible technique. *Opt. Mater.* **2017**, *64*(Suppl. C), 524-532.
18. Lipatova, Z. O., Kolobkova, E. V. Sidorov A. I.; Nikonorov, N. V. The influence of sodium nanoparticles formation on luminescent properties of fluorophosphate glasses containing molecular clusters and quantum dots of lead selenide. *Optics and Spectroscopy* **2016**, *121*, 200-209.
19. Yang, J., H.; Liu, H.; Yu, X.; Zou, B.; Jing, Dai (2016). Rheological behavior of a novel organic inorganic hybrid: Micro/nano-tin fluorophosphate glass-polycarbonate. *J. Nanosci. Nanotechnol.* **2016** *16*, 2677-2681.

20. Shaharyar, Y., Wein, E.; Kim, J.-J. Youngman, R. E. Munoz, F. Kim, H.- Tilocca, W.; Goel, A. (2015). Structure-solubility relationships in fluoride-containing phosphate based bioactive glasses. *J. Mater. Chem. B* **2015**, *3*, 9360-9373.
21. Brow, R. K.; Osborne, Z. A.; Kirkpatrick, R. J. A multinuclear MAS NMR study of the short-range structure of fluorophosphate glass. *J. Mater. Res*. **1982**, ***7***, 1892-1899.
22. Videau, J.-J., Portier, J.; Piriou, B. Raman spectroscopic studies of fluorophosphate glasses. *J. Non-Cryst. Solids* **1982**, *48*, 385-392.
23. Gan, F., Jiang, Y.; Jiang, F. Formation and structure of $Al(PO_3)_3$-containing fluorophosphate glass. *J. Non-Cryst. Solids* **1982**, *52*, 263-273.
24. Brow, R. K.; Osborne, Z. A. XPS studies of fluorine bonding in phosphate glasses. *Surf. Interface Anal.* **1996**, *24***,** 91-94.
25.Brow, R. K., Phifer, C.C.; Xu, X. J.; Day. D.E. An X-ray photoelectron spectroscopy study of anion bonding in tin(II) fluorophosphate glass. Phys. Chem. Glasses **1992**, *33*, 33-39.
26. Möncke, D., Ehrt, D.; Velli, L.L.; Varsamis, C. P. E.; Kamitsos, E.I. Structural investigations of fluoride phosphate glasses. *Proc. XX Int. Congr. Glass* **2004**, *P-10-030*, 1-6.
27. Möncke, D., Ehrt, D.; Velli, L. L.; Varsamis, C. P. E.; Kamitsos, E.I. Structure and properties of mixed phosphate and fluoride glasses. *Phys. Chem. Glasses* **2005**, *46***,** 67-71.
28. Möncke, D., Ehrt, D.; Velli, L. L.;Varsamis, C. P. E.; Kamitsos, E.I.; Elbers, S.; Eckert, H. Comparative spectroscopic investigation of different types of fluoride phosphate glasses. *Phys. Chem. Glasses - Eur. J. Glass Sci. Technol.* Part B **2007**, *48*, 399-402.
29. Le, Q. H., Palenta, T.; Benzine, O.; Griebenow, K.; Limbach, R.; Kamitsos, E.I.; Wondraczek, L. Formation, structure and properties of fluoro-sulfo-phosphate poly-anionic glasses. *J. Non-Cryst. Solids* **2017**, *477*, 58-72.
30. Jäger, C.; Ehrt, D.; Haubenreisser, U. Investigations of solid-state reactions of binary polyphosphate fluoride systems by means of thermal-analysis, X-ray diffraction and NMR-spectroscopy. 1. System $Ba(PO_3)_2$+BaF_2. *Z. Phys. Chem. NF* **1988**, *159*, 75-87.
31. Eckert, H. Structural characterization of noncrystalline solids and glasses using solid state NMR. *Prog. Nucl. Magn. Reson. Spectrosc*. **1992**, *24*, 159-293.
32. Gullion, T. Measurement of heteronuclear dipolar interactions by rotational-echo, double-resonance nuclear magnetic resonance. *Magn. Reson. Rev* **1997**, *17*, 83-131.
33. Gullion, T.; Schaefer, J. Rotational-echo double-resonance NMR. *J. Magn. Reson.* **1989**, *81***,** 196-200.
34. Eckert, H., Elbers, S.; Epping, J. D.; Janssen, M.; Kalwei, M.; Strojek, W.; Voigt, U. Dipolar solid-state NMR approaches towards medium-range structure in oxide glasses, in *New Techniques in Solid-State NMR*, Klinowski, J., ed., Springer Berlin Heidelberg**, 2005**, 195-233,
35. de Oliveira Jr. M., Goncalves, T. S.; Ferrari, C.; Magon, C. J.; Pizani, P. S.; de Camaro, A. S. S.; Eckert, H. Structure-property relations in fluoride phosphate glasses: An integrated spectroscopic strategy" *J. Phys. Chem*. C. **2017**, 121, 2968-2986.
36. de Oliveira Jr., M.; Uesbeck, T.; Gonçalves, T. S.; Magon, C. J. Pizani, P. S. de Camargo, A. S. S.; Eckert, H. Network structure and rare-earth ion local environments in fluoride phosphate photonic glasses studied by solid-state NMR and electron paramagnetic resonance Sspectroscopies. *J. Phys. Chem.* C **2015**, *119*, 24574-24587.
37. Body, M.; Legein, C.; Silly, G.; Buzaré, J. Y. ^{19}F high speed MAS NMR investigation of AlF_6^{3-} octahedron connectivity in fluoroaluminate glasses. *J. Non-Cryst. Solids* **2007**, 353**,** 2231-2236.
38. Ebendorff-Heidepriem, H.; Ehrt, D. "Determination of the OH content of glasses " *Glastechn. Ber.-Glass Sci. Technol.* **1995**, *68*, 139-146.

39. Ehrlich, P.; Pietzka G. Die maßanalytische Bestimmung des Fluors nach Fällung als Bleibromofluorid. *Fresenius' Z. Anal. Chem*. **1951**, *133*, 84-94.
40. Lesage, A.; Bardet, M.; Emsley, L. Through-bond carbon−carbon connectivities in disordered solids by NMR *J. Am. Chem. Soc.* **1999,** *121*, 10987-10993.
41. Cadars, S.; Sein, J.; Duma, L.; Lesage, A.; Pham, T.N.; Baltisberger, J.H.; Brown, S. P.; Emsley, L. The refocused INADEQUATE experiment in multiple spin-systems: Interpreting observed correlation peaks and optimising lineshapes. *J Magn Reson*. **2007**, 188, 24-34.
42. Chan, J. C. C.; Eckert, H. Dipolar coupling information in multispin systems: Application of a compensated REDOR NMR approach to inorganic phosphates. *J. Magn. Reson.* **2000**, *147*, 170-178.
43. Zhang, L., de Araujo, C. C.; Eckert, H. Structural role of fluoride in aluminophosphate sol−gel glasses: High-resolution double-resonance NMR studies. *J. Phys. Chem. B* **2007**, *111*, 10402-10412.
44. Czjzek
45. Zhang, L.; Eckert. H. Short- and medium-range order in sodium aluminophosphate glasses: New insights from high-resolution dipolar solid-state NMR spectroscopy. *J. Phys. Chem. B* **2006**, *110*, 8946-8958.
46. Van Vleck, J. H. The dipolar broadening of magnetic resonance lines in crystals. *Phys. Rev*. **1948**, *74*,1168-1183.
47. Durand, J.; Le Cot, L.; Galigne, J. L. Etudes structurales de compos6s oxyfluor6s du P(V) II. Structure cristalline de Na_2PO_3F *Acta Crystallogr. Sec.B. Struct. Crystallogr. Cryst. Chem*. **1974**, *30*, 1565-1569.
48. Jost, K. H. Die Struktur des Kurrol'schen Na-Salzes $(NaPO_3)_x$, Typ B, *Acta Crystallogr*. **1963** *16*, 640-642.
49. Wyckoff, R.W.G. Crystal Structures **1963**, *1*, 85-237.
50. Strojek, W.; Kalwei, M.; Eckert, H. "Dipolar NMR strategies for multispin systems involving quadrupolar nuclei: $^{31}P\{^{23}Na\}$ rotational echo double resonance (REDOR) of crystalline sodium phosphates and phosphate glasses." *J. Phys. Chem. B* **2004**, *108*, 7061-7073.
51. Bak, M., Rasmussen, J. T.; Nielsen, N. C. SIMPSON: A general simulation program for solid-state NMR spectroscopy. *J. Magn. Reson*. **2000,** *147*, 296-330.
52. P. Daniel, A. Bulo, M. Rousseau, J. Nouet, J. L. Fourquet, M. Leblanc, R. Burriel, A Study of the structural phase transitions in AlF_3: X-ray powder diffraction, differential scanning calorimetry (DSC) and Raman scattering investigations of the lattice dynamics and phonon spectrum, *J. Phys. Cond. Matter*, **1990**, *2*, 5663-5677.
53. Pauling, L.; Sherman, J. Structure of aluminum metaphosphates, *Z. Kristallographie, Kristallgeometrie, Kristallphysik, Kristallchemie* **1937**, *96*, 481-487.
54. Ehrt, D.; Jäger, C. Investigations of solid-state reactions of binary polyphosphate fluoride systems by means of thermal analysis, X-ray diffraction and NMR spectroscopy. IV. Systems $M(PO_3)_3$+MF_3 (M=Al, La). *Z. Phys. Chem. NF* **1989**, *162*, 97-107
55. Ehrt, D.; Jäger, C. Investigations of solid-state reactions of binary polyphosphate fluoride systems by means of thermal analysis, X-ray diffraction and NMR spectroscopy. VI. Reactions of $Mg(PO_3)_2$, $Ba(PO_3)_2$ and $La(PO_3)_3$ with an excess of AlF_3. *Z Phys. Chem. NF* **1989**, *165*, 55-65

SUPPORTING MATERIALS SECTION

Structural Studies of $NaPO_3$-AlF_3 Glasses by High-Resolution Double-Resonance NMR Spectroscopy

Henrik Bradtmüller[a], Long Zhang [a,b], Carla C. de Araujo[a], Hellmut Eckert [a,c*], Doris Möncke[d] and Doris Ehrt[e]

[a] Institut für Physikalische Chemie, Westfälische Wilhelms-Universität Münster, Corrensstr. 30, D-48149 Münster, Germany

[b] Shanghai Institute of Optics and Fine Mechanics, Chinese Academy of Sciences, P. O. Box: 800-211, 201800 Shanghai, China

[c] Instituto de Física São Carlos, Universidade de São Paulo, CP 369, São Carlos, SP 13566-590

[d] Theoretical and Physical Chemistry Institute, National Hellenic Research Foundation, 48 Vassileos Constantinou Avenue, 11635 Athens, Greece

[e] Otto-Schott-Institut, Friedrich-Schiller-Universität Jena, Fraunhoferstr 6, D-07743 Jena, Germany

[*] Author to whom correspondence should be addressed.

Phone: 49-251-8329161; Fax: 49-251-8329159; E-mail: eckerth@uni-muenster.de.

2. NMR METHODOLOGY

The experimental strategy employed in the present study includes the quantitative analysis of high-resolution ^{19}F, ^{23}Na, ^{27}Al and ^{31}P NMR solid-state NMR spectra in conjunction with a quantitative analysis of their internuclear magnetic dipole-dipole interactions. Figure S1 shows the two $S\{I\}$ REDOR pulse sequences used in the present study.[1-3] A normalized difference signal $\Delta S/S_0 = (S_0\text{-}S)/S_0$ is measured in the absence (intensity S_0) and the presence (intensity S) of the dipolar interactions between the observed nuclei S and the second nuclear species I.

Determination of $\Delta S/S_0$ under systematic variation of the number of rotor cycles N yields the so-called REDOR curve, in which the data are plotted as a function of dipolar evolution time NT_r (T_r being the duration of one rotor period). For isolated spin-1/2 pairs these curves possess a universal shape, allowing straightforward determination of the magnetic dipole-dipole coupling constant.[32,33] In contrast, the analysis of $S\{I\}$ REDOR curves in inorganic glasses is complicated by multispin interactions, distance distributions and interference by nuclear electric quadrupolar couplings. We have previously shown that in the case of $S\{I\}$ REDOR experiments with $I = 1/2$ nuclei, the problem can be simplified by confining the REDOR data analysis to the initial curvature, where $\Delta S/S_0 \leq 0.2$.[4,5] In this limit the REDOR curve is found to be independent of specific spin system geometries, and can be approximated by a simple parabola:

$$\frac{\Delta S}{S_0} = \frac{4}{3\pi^2} M_2^{SI} \left(NT_r\right)^2 \qquad (1)$$

From the curvature of this parabola we can determine the van-Vleck second moment[6] $M_{2(\text{S-I})}$, a quantity that can be used to characterize the average dipole-dipole coupling strengths the S nuclei experience from the magnetic moments of their neighboring I nuclei. The approach yields satisfactory results also in amorphous and strongly disordered systems where the order and geometry of the spin systems is unknown and possibly ill-defined.

In those cases, where the dipolar dephasing of the observed spins occurs in the local field of $I > 1/2$ nuclei such as ^{23}Na ($I = 3/2$) several additional complications enter. First of all, the different possible Zeeman states m_I for the I nuclei differ in the respective sizes of their z components and hence generate dipolar fields of different magnitudes at the observed spins. Secondly, for strong nuclear electric quadrupolar coupling, the anisotropic broadening of the $|1/2\rangle \leftrightarrow |3/2\rangle$ "satellite transitions" produces large resonance offsets, which reduce the efficiency of π pulses in causing population inversion. In the limit of very large first-order quadrupolar

splitting (rf nutation frequency $\nu_1 << C_Q$, the quadrupolar coupling constant), pulses applied to the *I* nuclei in the REDOR sequences will affect only the central |1/2> ↔ |-1/2> coherences. In this regime only those *S* spins that are coupled to *I* nuclei in Zeeman states with $|m_I| = 1/2$ are expected to yield a REDOR response. Detailed simulations have led to the conclusion that it is desirable in such cases to minimize the number of π pulses applied to the quadrupolar nuclei, making the REDOR sequence of Figure S1b the method of choice. As we have previously shown,[7] the initial curvature analysis discussed above can be extended to systems containing $I = 3/2$ nuclei by using the expression

$$\frac{\Delta S}{S_0} = \frac{1}{15\pi^2}(2+18f_1)M_2^{SI}\left(NT_r\right)^2 \qquad (2)$$

where the efficiency factor f_1 ($0 \le f_1 \le 1$) accounts for the extent to which the dipolar coupling of *S* spins to *I* spins in their outer Zeeman states still influences the REDOR response. Again, Eq. (2) is valid for the initial regime ($0 \le \Delta S/S_0 \le 0.2$) only. The whole data analysis procedure for this particular case can be summarized as follows: Based on the nuclear electric quadrupolar coupling Hamiltonian parameters determined experimentally, a universal REDOR curve is computed (using the SIMPSON code[8]) based on explicitly those experimental conditions under which the REDOR data were taken. This simulated curve is then fitted to (Eq. (2)), resulting in the appropriate f_1 value, which is then applicable for the analysis of the experimental data set. Using the f_1 value determined in this fashion, the experimental data are fitted to Eq. (2), resulting in an experimental second moment. This value can then be compared with calculations based on structural models using the well-known van Vleck equation:[6]

$$M_2^{SI} = \left(\frac{\mu_0}{4\pi}\right)^2 \frac{4}{15} I(I+1)\hbar^2\gamma_S^2\gamma_I^2\sum_S r_{IS}^{-6} \qquad (3)$$

where γ_I and γ_S are the gyromagnetic ratios of the nuclei *I* and *S* involved, and r_{IS} are the internuclear distances. In the present study, we will use this approach to analyze the dipolar field created by ^{23}Na at the observed ^{31}P and ^{19}F nuclei.

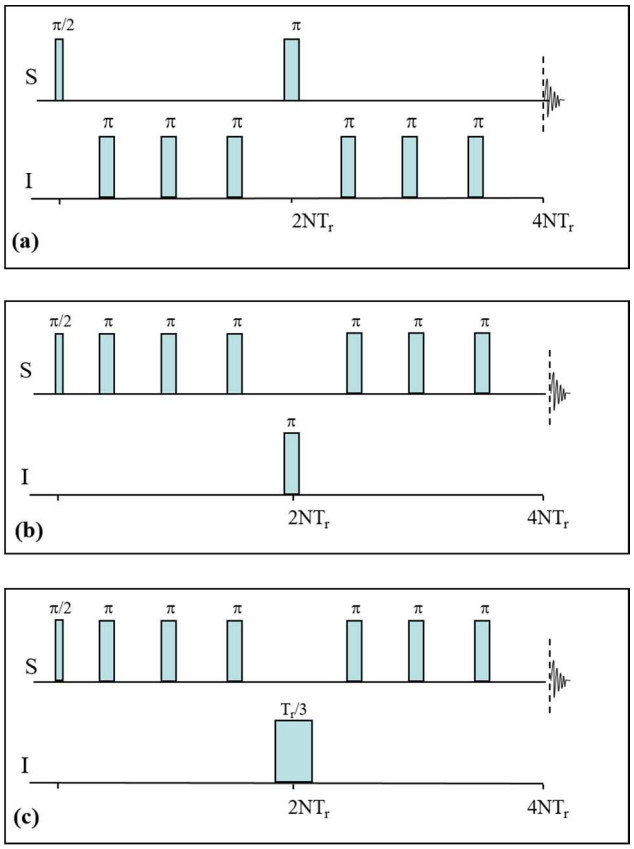

Figure S1: NMR pulse sequences used in the present study. a) sequence used for S{I} REDOR, $I = 1/2$; b) sequence used for S{I} REDOR, $I = 3/2$; c) a related method, called Rotational Echo Adiabatic Passage Double Resonance (REAPDOR), in which a pulse of a duration of 1/3 of the rotor period is applied to the quadrupolar I nuclei.

Table S1. Experimental conditions used in the double resonance NMR experiments

REDOR experiment	ν_0(S) [a] (MHz)	ν_0(I) [b] (MHz)	$\tau_{90°}$(S) [c] (μs)	$\tau_{90°}$(I) [d] (μs)	R [f] (s)	NS [g]
^{27}Al{^{19}F}	130.3	470.4	2.5	2.2	2	128-512
^{27}Al{^{31}P}	104.3	162.0	3.0	3.0	2	256
^{19}F{^{31}P}	470.4	202.5	2.2	3.0	10	128-256
^{19}F{^{23}Na}	470.4	132.3	2.2	1.8	10	128-256
^{23}Na{^{19}F}	132.3	470.4	1.8	1.4	2	128-512
^{23}Na{^{31}P}	158.8	243.0	1.7	1.7	1	256
^{31}P{^{23}Na}	162.0	105.9	3.0	3.0	60	64
^{31}P{^{27}Al} [h]	242	156.4	1.8	- [i]	350	112
^{31}P{^{19}F} [h]	98	228.0	2.0	4.0	350	112

S-spin resonance frequency. [b] I-spin resonance frequency. [c] S-spin-90° pulse length. [d] I-spin-90° pulse length. [f] Relaxation delay. [g] Number of scans. [h] single-point experiments. [i] Adiabatic pulse of 16.7 μs (1/3 rotor period) was employed.

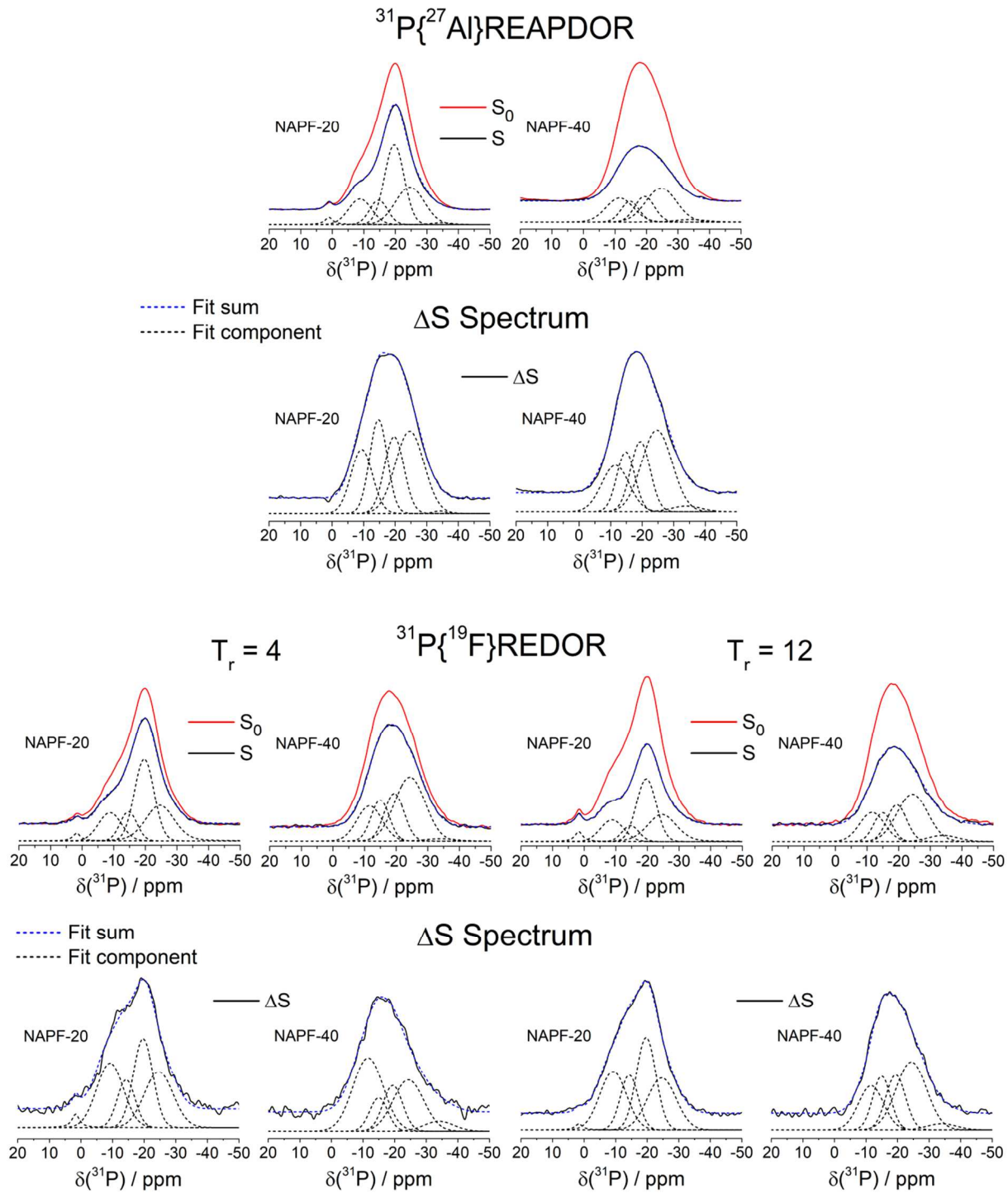

Figure S2: $^{31}P\{^{19}F\}$ REDOR and $^{31}P\{^{27}Al\}$ REAPDOR spectra S_0, Hahn-Echo spectra S and calculated difference spectra ΔS of NAPF-20 and NAPF-40 glasses. Deconvolutions are shown for S_0 and ΔS spectra and use pure Gaussian lines with identical chemical shifts and widths. A dipolar mixing time of 12 rotor cycles was employed for REDOR and REAPDOR experiment.

Table S2: Deconvolution parameters of $^{31}P\{^{19}F\}$ REDOR and $^{31}P\{^{27}Al\}$ REAPDOR spectra.

Sample	δ_{CS}^{iso} (^{31}P) / ppm	FWHM / ppm	Area fractions / %			
			$^{31}P\{^{19}F\}$ REDOR		$^{31}P\{^{27}Al\}$ REAPDOR	
			S	ΔS	S	ΔS
$80NaPO_3$-$20AlF_3$						
1[a]	1.7	2.9	4	1	2	-
2	-8.8	8.5	17	26	15	20
3	-14.7	6.3	9	17	12	24
4	-19.7	7.3	41	31	41	22
5	-24.6	10.7	29	25	29	34
6	-34.6	7.3	-	-	1	<1
$60NaPO_3$-$40AlF_3$						
1	-11.6	9.3	20	20	25	20
2	-15.0	6.7	14	18	14	17
3	-19.4	7.3	20	20	19	22
4	-24.3	11.4	41	39	39	39
5	-34.0	11.0	5	3	3	3

[a] Purely Lorentzian line shape

Table S3: First fifteen Na-F distances of the four sodium sites in crystalline Na_2PO_3F and their Na-F second moments. The effective M_2 is shown below for each site and considers distances up to five times the shortest Na-F distance. The effective distance expresses the calculated value of $M_{2(Na\text{-}F)}$ in a single Na-F spin-pair.

# Na-F	d(Na-F) / □				# Na-F	$M_{2(Na\text{-}F)}$ / 10^6rad^2/s^2			
	Na1	Na2	Na3	Na4		Na1	Na2	Na3	Na4
1	2.30	2.30	3.52	2.66	1	48.0	48.0	3.7	20.0
2	3.40	3.42	4.02	3.00	2	4.6	4.4	1.7	9.7
3	3.85	3.55	4.53	3.20	3	2.2	3.5	0.8	6.6
4	4.02	4.15	4.54	3.21	4	1.7	1.4	0.8	6.5
5	4.64	4.65	4.55	3.31	5	0.7	0.7	0.8	5.4
6	5.48	5.55	4.63	4.80	6	0.3	0.2	0.7	0.6
7	5.56	5.58	4.69	5.33	7	0.2	0.2	0.7	0.3
8	5.62	5.74	4.79	5.88	8	0.2	0.2	0.6	0.2
9	5.74	5.84	4.87	6.19	9	0.2	0.2	0.5	0.1
10	5.78	5.86	4.99	6.40	10	0.2	0.2	0.5	0.1
11	5.81	5.88	5.00	7.00	11	0.2	0.2	0.5	0.1
12	5.89	6.02	6.17	7.05	12	0.2	0.1	0.1	0.1
13	6.00	6.20	6.23	7.13	13	0.2	0.1	0.1	0.1
14	6.10	6.59	6.68	7.33	14	0.1	0.1	0.1	0
15	6.10	6.74	6.96	7.34	15	0.1	0.1	0.1	0
Effective	2.21	2.21	2.87	2.28	Sum	60.0	60.1	12.6	50.8

Table S4: First fifteen Na-P distances of the four sodium sites in crystalline Na_2PO_3F and their contributions to Na-P second moments. The effective M_2 is shown below for each site and considers distances up to five times the shortest Na-P distance. The effective distance expresses the calculated M_2 in a single Na-P spin-pair.

# Na-P	*d*(Na-P) / □				# Na-P	$M_{2(Na-P)}$ / 10^6rad^2/s^2			
	Na1	Na2	Na3	Na4		Na1	Na2	Na3	Na4
1	3.08	3.13	3.39	3.47	1	1.54	1.40	0.86	0.75
2	3.15	3.18	3.46	3.47	2	1.33	1.26	0.76	0.75
3	3.18	3.30	3.55	3.48	3	1.26	1.02	0.65	0.74
4	3.24	3.37	3.73	3.50	4	1.13	0.90	0.48	0.71
5	3.88	3.74	3.89	3.59	5	0.39	0.48	0.38	0.61
6	5.86	5.88	3.93	3.86	6	0.03	0.03	0.36	0.39
7	6.07	5.92	5.88	5.88	7	0.03	0.03	0.03	0.03
8	6.15	6.06	5.91	5.94	8	0.02	0.03	0.03	0.03
9	6.21	6.08	5.95	6.13	9	0.02	0.03	0.03	0.02
10	6.24	6.18	6.00	6.18	10	0.02	0.02	0.03	0.02
11	6.33	6.20	6.10	6.23	11	0.02	0.02	0.03	0.02
12	6.41	6.39	6.12	6.42	12	0.02	0.02	0.03	0.02
13	6.54	6.44	6.15	6.44	13	0.02	0.02	0.02	0.02
14	6.55	6.48	6.45	6.44	14	0.02	0.02	0.02	0.02
15	6.65	6.54	6.50	6.45	15	0.02	0.02	0.02	0.02
Effective	2.45	2.49	2.63	2.59	Sum	6.1	5.5	3.9	4.4

Table S5: First fifteen Na-P distances of the two sodium sites in crystalline $NaPO_3$ and their contributions to Na-P second moments. The effective M_2 is shown below for each site and considers distances up to five times the shortest Na-P distance. The effective distance expresses the calculated M_2 in a single Na-P spin-pair.

# Na-P	*d*(Na-P) / □		# Na-P	$M_{2(Na-P)}$ / 10^6rad^2/s^2	
	Na1	Na2		Na1	Na2
1	3.19	3.13	1	1.24	1.39
2	3.24	3.28	2	1.12	1.06
3	3.54	3.32	3	0.66	0.98
4	3.56	3.32	4	0.65	0.97
5	3.59	3.45	5	0.61	0.77
6	3.81	3.93	6	0.43	0.36
7	4.51	4.73	7	0.16	0.12
8	4.60	4.74	8	0.14	0.12
9	4.93	4.93	9	0.09	0.1
10	5.30	5.37	10	0.06	0.05
11	5.40	5.49	11	0.05	0.05
12	5.83	5.63	12	0.03	0.04
13	5.83	5.77	13	0.03	0.04
14	5.94	5.87	14	0.03	0.03
15	6.19	6.00	15	0.02	0.03
Effective	2.48	2.42	Sum	5.7	6.4

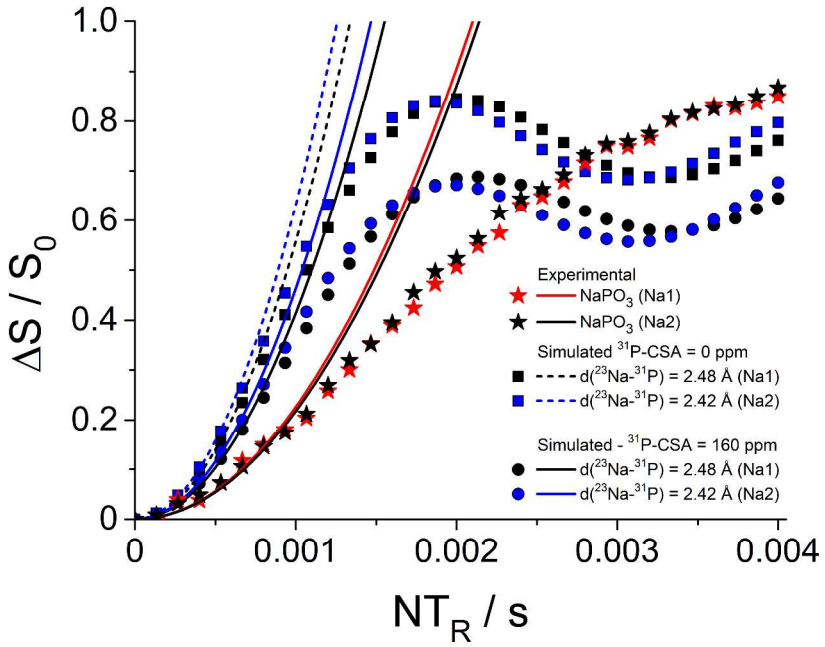

Figure S4: Experimental and simulated ^{23}Na{^{31}P} REDOR curves obtained on crystalline $NaPO_3$. Simulations represent the behavior of a ^{23}Na-^{31}P two-spin system with and without the influence of the ^{31}P chemical shift anisotropy (CSA). The dipolar interaction strength for the simulation was calculated from the distance sum of all ^{23}Na-^{31}P spin pairs within 25 □, according to the two Na-sites found in crystalline $NaPO_3$.

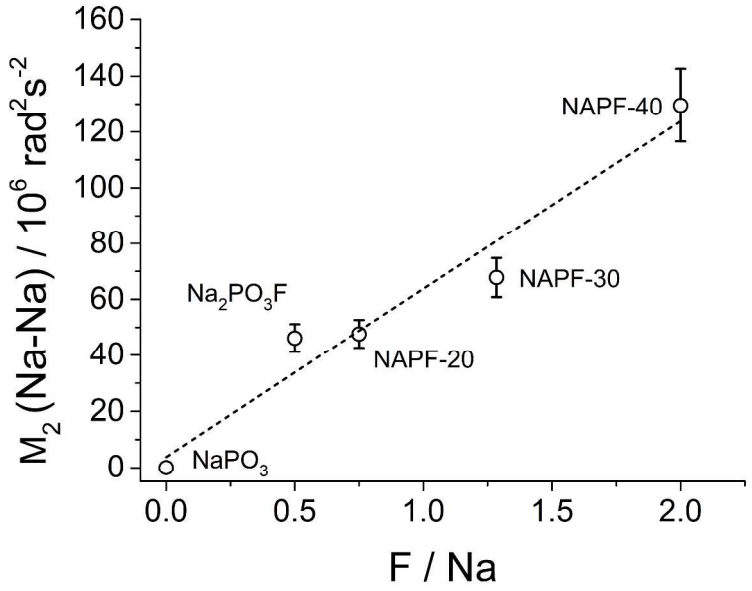

Figure S5: Linear correlation model of experimental $M_{2(Na\text{-}F)}$ values obtained from ^{23}Na{^{19}F} REDOR, versus the F to Na ratio for $NaPO_3$ (hypothetically. M_2=0 rad^{2}s^{-2}), crystalline Na_2PO_3F and the studied glasses. R^2 = 0.944, ordinate 3.8 rad^{2}s^{-2}, slope 60.0 rad^{2}s^{-2}.

REFERENCES

1. Gullion, T. Measurement of Heteronuclear Dipolar Interactions by Rotational-echo, Double-resonance Nuclear Magnetic Resonance. *Magn. Reson. Rev* **1997**, *17*, 83-131.
2. Gullion, T.; Schaefer, J. Rotational-echo Double-resonance NMR. *J. Magn. Reson.* **1989**, *81***,** 196-200.
3. Eckert, H., Elbers, S.; Epping, J. D.; Janssen, M.; Kalwei, M.; Strojek, W.; Voigt, U. Dipolar Solid State NMR Approaches Towards Medium-Range Structure in Oxide Glasses, in *New Techniques in Solid-State NMR*, Klinowski, J., ed., Springer Berlin Heidelberg**, 2005**, 195-233,
4. Bertmer, M. and H. Eckert "Dephasing of Spin Echoes by Multiple Heteronuclear Dipolar Interactions in Rotational Echo Double Resonance NMR Experiments. *Solid State Nucl. Magn. Reson*. **1999**, *15*, 139-152.
5. Chan, J. C. C.; Eckert, H. Dipolar Coupling Information in Multispin Systems: Application of a Compensated REDOR NMR Approach to Inorganic Phosphates. *J. Magn. Reson.* **2000**, *147*, 170-178.
6. Van Vleck, J. H. The Dipolar Broadening of Magnetic Resonance Lines in Crystals. *Phys. Rev*. **1948**, *74*,1168-1183.
7. Strojek, W.; Kalwei, M.; Eckert, H. "Dipolar NMR Strategies for Multispin Systems Involving Quadrupolar Nuclei: $^{31}P\{^{23}Na\}$ Rotational Echo Double Resonance (REDOR) of Crystalline Sodium Phosphates and Phosphate Glasses." *J. Phys. Chem*. *B* **2004**, *108*, 7061-7073.
8. Bak, M., Rasmussen, J. T.; Nielsen, N. C. SIMPSON: A General Simulation Program for Solid-State NMR Spectroscopy. *J. Magn. Reson*. **2000,** *147*, 296-330.